


Increased myocellular lipid and IGFBP-3 expression in a pre-clinical model of pancreatic cancer-related skeletal muscle wasting

Calvin L. Cole^{1,2,3,4,5*} , John F. Bachman^{6,7}, Jian Ye³, Joseph Murphy³, Scott A. Gerber^{3,5,8,9}, Christopher A. Beck^{1,2,10}, Brendan F. Boyce^{2,5}, Gowrishankar Muthukrishnan^{1,2}, Joe V. Chakkalal^{2,7,5}, Edward M. Schwarz^{1,2,5} & David Linehan^{3,5}

¹Department of Orthopaedics, University of Rochester Medical Center, Rochester, New York, USA; ²Center for Musculoskeletal Research, University of Rochester Medical Center, Rochester, New York, USA; ³Department of Surgery, University of Rochester Medical Center, Rochester, New York, USA; ⁴Division of Supportive Care in Cancer, University of Rochester Medical Center, Rochester, New York, USA; ⁵Wilmot Cancer Institute, University of Rochester Medical Center, Rochester, New York, USA; ⁶Department of Pathology and Laboratory Medicine, University of Rochester Medical Center, Rochester, New York, USA; ⁷Department of Pharmacology & Physiology, University of Rochester Medical Center, Rochester, New York, USA; ⁸Department of Microbiology & Immunology, University of Rochester Medical Center, Rochester, New York, USA; ⁹Department of Radiation Oncology, University of Rochester Medical Center, Rochester, New York, USA; ¹⁰Department of Biostatistics and Computational Biology, University of Rochester Medical Center, Rochester, New York, USA

Abstract

Background Skeletal muscle wasting (SMW) in cancer patients is associated with increased morbidity, mortality, treatment intolerance and discontinuation, and poor quality of life. This is particularly true for patients with pancreatic ductal adenocarcinoma (PDAC), as over 85% experience SMW, which is responsible for ~30% of patient deaths. While the established paradigm to explain SMW posits that muscle catabolism from systemic inflammation and nutritional deficiencies, the cause of death, and the cellular and molecular mechanisms responsible remain to be elucidated. To address this, we investigated the relationship between tumour burden and survival in the KCKO murine PDAC model.

Methods Female C57BL/6J mice 6–8 weeks of age underwent orthotopic injection with KCKO-luc tumour cells. Solid tumour was verified on Day 5, post-tumour inoculation. *In vivo*, longitudinal lean mass and tumour burden were assessed via dual-energy X-ray absorptiometry and IVIS imaging, respectively, and total body weight was assessed, weekly. Animals were sacrificed at a designated end point of ‘failure to thrive’. After sacrifice, lower limb hind muscles were harvested for histology and RNA extraction.

Results We found a strong correlation between primary tumour size and survival ($r^2 = 0.83$, $P < 0.0001$). A significant decrease in lower limb lean mass was first detected at Day 38 post-implantation vs. no tumour controls (NTCs) ($P < 0.0001$). SMW was confirmed by histology, which demonstrated a 38%, 32.7%, and 39.9% decrease in fibre size of extensor digitorum longus, soleus, and tibialis anterior muscles, respectively, in PDAC mice vs. NTC ($P < 0.002$). Histology also revealed a 67.6% increase in haematopoietic cells within the muscle of PDAC mice when compared with NTC. Bulk RNAseq on muscles from PDAC mice vs. NTC revealed significant increases in *c/ebpβ/Δ*, *il-1*, *il-6*, and *tnf* gene expression. Pathway analyses to identify potential upstream factors revealed increased adipogenic gene expression, including a four-fold increase in *igfbp-3*. Histomorphometry of Oil Red-O staining for fat content in tibialis anterior muscles demonstrated a 95.5% increase in positively stained fibres from PDAC mice vs. NTC.

Conclusions Together, these findings support a novel model of PDAC-associated SMW and mortality in which systemic inflammation leads to inflammatory cell infiltration into skeletal muscle with up-regulated myocellular lipids.

Keywords Myocellular lipid; Murine model; Pancreatic cancer; Skeletal muscle wasting

Received: 17 December 2020; Revised: 16 February 2021; Accepted: 15 March 2021

*Correspondence to: Calvin L. Cole, PhD, Department of Orthopaedics, University of Rochester Medical Center, 601 Elmwood Avenue, Box 665 Rochester, NY 14642, USA. Phone: 585-276-5976, Fax: 585-276-2177, Email: calvin_cole@urmc.rochester.edu

Introduction

Sarcopenia, also known as skeletal muscle wasting (SMW), is a progressive and generalized skeletal muscle disorder, associated with an increased likelihood of adverse outcomes including falls, fractures, physical disability, poor quality of life, and mortality.¹ SMW has been identified as a prognostic factor in pancreatic ductal adenocarcinoma (PDAC),² and is an independent predictor of infectious complications and post-operative mortality.^{3,4} It is also associated with adverse postoperative outcomes, treatment toxicity, increased length of hospital stay, and poor recovery in patients with pancreatic cancer.^{5,6} Thus, SMW is particularly problematic for PDAC patients, as improvement in treatment tolerance in this population is vital given the very low 5-year survival rate (<10%).⁷ In addition, among cancer patients, the prevalence of SMW is highest in those with PDAC. In fact, over 85% of patients with PDAC experience SMW, which contributes significantly to mortality, where nearly 30% of patient's deaths are attributable to loss of lean mass, rather than an advanced tumour burden.⁸ Thus, it has been argued that development of interventions for SMW are as important as treating the cancer itself.⁹

Currently, surgical resection is the only treatment with curative intent for PDAC. However, because of the aggressive nature of the disease and high probability of recurrence and metastasis, combination therapy with surgery and chemotherapy are recommended as standard of care for resectable patients.¹⁰ In these patients, SMW is associated with high-grade complications, increased time in the hospital and intensive care, and reduced likelihood of adjuvant therapy.¹⁰ Therefore, treatments for SMW may improve treatment outcomes, quality of life, and survival in patients with PDAC. There remains a need for pre-clinical models of PDAC-related SMW that recapitulate clinical disease and can be assessed longitudinally to investigate pathologies associated with its initiation and progression and find effective therapies.

Although current knowledge of the aetiology of PDAC-associated SMW is limited, a fundamental framework of its initiation and progression has been established.¹¹ Based on the anatomical distance between primary tumour and sites of SMW, the established paradigm posits that tumour-derived factors act as paracrine factors to initiate proteolysis via inhibition of myofibrillar protein synthesis and accelerated muscle catabolism.^{11,12} Indeed, cancer and its treatments have been shown to cause a systemic increase in tumour necrosis factor- α (TNF- α), interleukin-1 (IL-1), and interleukin-6 (IL-6) in both humans and animal models of PDAC-related SMW,^{11,13} and these have also been linked to decreased survival in this population. These cytokines are secreted by PDAC tumour and infiltrating immune cells that are activated in response to the tumour burden.^{14,15} Immune cells such as tumour-associated macrophages (TAMs),

inflammatory monocytes, and myeloid-derived suppressor cells are known to play an immunosuppressive role during PDAC tumour development and growth through inhibition of cytotoxic T cells.^{16,17} Furthermore, TAMs secrete pro-inflammatory cytokines, such as TNF- α , IL-1, and IL-6.¹⁶ Systemic consequences include infiltration of these immune cells into muscle tissue,¹⁶ leading to a local up-regulation of pro-inflammatory cytokines and muscle catabolism.^{11,14} However, pre-clinical studies and clinical trials with cytokine inhibitors have failed to demonstrate significant inhibition of PDAC-associated SMW,¹¹ suggesting a great redundancy that would require inhibition of many pleiotropic pro-inflammatory cytokines, and/or a yet to be identified paracrine pathway that controls this catastrophic process.

To elucidate the mechanism of PDAC-related SMW in mice, we have utilized the *Muc1*-null PDAC model (designated KCKO).¹⁷ We chose this model because lack of *Muc1* significantly decreases proliferation, invasion, and mitotic rates of the tumour cells both *in vivo* and *in vitro*, compared with PDAC cells containing *Muc1* (designated KC and KCM).¹⁸ Furthermore, in the absence of *Muc1*, the pancreatic tumour burden and secondary metastases are decreased. This feature provides KCKO tumour-bearing mice a significant survival benefit compared with KC and KCM mice,¹⁸ and this is critical for studies of SMW. We have also shown that KCKO mice live >5 weeks longer than KC mice, which provides an enhanced opportunity for therapeutic intervention before, during, and after the onset of PDAC-related SMW.¹⁹ We acknowledge the existence of orthotopic²⁰ and genetic models²¹ of PDAC that experience similar degrees of muscle loss to that of our model and that these models have been utilized to assess potential treatments. However, limitations of these models have been noted. While Mulder *et al.* showed efficacy in targeting c-Jun N-terminal kinase (JNK) to attenuate SMW in an orthotopic model of PDAC, they did so in an immune incompetent mouse.²⁰ Although this research was effective in showing the impact of such a treatment on a specific target, it has limited clinical translation because it is impossible to understand the consequence(s) that inhibiting JNK has on immune response. It is important to understand the affect that treatments for cancer-related SMW have on host immunity due to the known relationship that exist between an up-regulated immune response and proteolysis. It is also important to note the distinction between muscle wasting caused by distal metastasis vs. local progression. Talbert *et al.* provide a compelling rationale for the use of *Kras*^{G12D}, *Ptf1a*^{+ER-Cre}, *Pten*^{f/f} (KPP) mice to study SMW.²¹ The KPP model of PDAC capitalizes on the limitations of other PDAC genetic models in that it can be initiated in young and older adult mice. This characteristic of the KPP model increases the likelihood that muscle wasting is induced after the rapid neonatal growth of mice has concluded.²¹ Although there are benefits to using this PDAC model, we found that the orthotopic KCKO model was more appropriate because

it allows for the synchronization of the onset of disease and disease progression. Also, five injections of tamoxifen are needed to activate the CRE recombinase in the KPP model. The use of tamoxifen would be a contraindication in our model, as it has been found to induce the secretion of IGFBP-3.²² Furthermore, the addition of luciferase to KCKO cells provides the opportunity to longitudinally assess tumour burden, which enables the assessment of the relationship among tumour burden, survival, and onset of SMW relative to disease.

To our knowledge, this is the first model of its kind and incorporates clinically translatable outcome measures. Most recently, we developed longitudinal DEXA outcome measures to quantify lean mass in KCKO mice and demonstrated that this PDAC model faithfully recapitulates the pathophysiology of cancer-related SMW.²³ Based on this advance, we aimed to determine the kinetics of SMW and its relationship to primary tumour size and mortality in the KCKO model. We also aimed to elucidate the cellular and molecular changes that occur in the skeletal muscle tissues of these mice with end-stage PDAC-associated SMW. Here, we report the results of these studies, which confirm the role of pro-inflammatory cytokines and immune cell infiltration and also identify a novel up-regulation of myocellular lipid accumulation within cachectic muscle fibres. Thus, this may be a unique pathology that triggers end-stage disease.

Materials and methods

Animals

Murine orthotopic model of pancreatic cancer

All experiments were approved by the University Committee on Animal Resources and were performed in compliance with the National Institutes of Health (NIH)-approved and University of Rochester-approved guidelines for the care and use of animals. We utilized the murine syngeneic-orthotopic model of PDAC, as previously described.²³ Briefly, female C57BL/6J mice 6–8 weeks of age were used. After a 1 week acclimation period, mice were randomized to one of two groups: PDAC or no tumour control (NTC). Mice in the PDAC group were anaesthetized and injected in the tail of the pancreas with 2×10^5 KCKO-luc cells suspended in a 1:1 phosphate-buffered saline (PBS) to Matrigel (Corning) mixture. NTC mice received no surgery and were sacrificed at a ratio of 1:1 with mice in the PDAC group. Mice were maintained in standard isolation cages with a 12 h light:dark cycle, and given ad libitum access to water and standard chow. Tumour-bearing mice were sacrificed when they developed end-stage disease, defined by having three or more characteristics of the Institutional Animal Care and Use Committee's (IACUC) definition of 'failure to thrive'. Characteristics of

'failure to thrive' included, but were not limited to self-isolation, hunched over appearance, lack of or reduced cage activity, lack of or no resistance to scruffing, mangled hair appearance after scruffing, failure to eat or drink, and/or visual signs of breathing difficulty. To determine if these characteristics developed, animals were checked twice daily, 30 days after tumour inoculation. This is the time point at which untreated animals reach an advanced stage of disease.²⁴ Mice in the non-tumour-bearing group were sacrificed contemporaneously to allow for intergroup comparisons. When animals were found to have three or more characteristics of 'failure to thrive', they were euthanized via ketamine overdose and secondary cervical dislocation.

Bioluminescent imaging

In vivo tumour growth was measured using an IVIS Spectrum Imaging System (IVIS, PerkinElmer). Mice were anaesthetized by vaporized isoflurane and injected subcutaneously (s.c.) with D-luciferin (2.5 mg, Invitrogen) in 100 ml PBS vehicle. While in the right lateral recumbent position, a series of images were taken at 2 min intervals for 24 min, and photon emissions were collected. Bioluminescence (p/s/cm²/sr) was calculated within matching (circular) regions of interest (ROIs) manually placed over tumours. Peak intensity was recorded for each tumour upon two sequential measurements demonstrating signal decay.

Dual-energy X-ray absorptiometry

This technique was performed as previously described.²³ Briefly, body composition was assessed in all mice using a dual-energy X-ray absorptiometry (DEXA) scanner. Mice were weighed before undergoing DEXA scanning. Each mouse was anaesthetized for the duration of the procedure (5 min). Mice were placed on the scanner bed in the prone position with limbs and tail stretched away from the body. Lean mass was calculated using the lower hind limbs as an ROI to exclude measurement of the tumour burden. For each mouse, lean mass was calculated for the lower right and left limb independently, and the average of both measurements was used as the final lean mass for the animal.

Tumour histology

All PDAC tissue samples were cut to 4 μ m and fixed in 10% neutral buffered formalin and processed through paraffin and sectioned in the University of Rochester, Center for Musculoskeletal Research Histology Core. Tumour sections (4 μ m thick) were placed on slides, deparaffinized and rehydrated in distilled water and stained in Mayers Haematoxylin for 4 min. Sections then were washed in tap water for 4–5 min, dipped in 0.3% acid alcohol, and washed three times in distilled water. Sections were then incubated in 1 \times PBS for 1 min, then washed three times in distilled water. Tissue was counterstained for 1 min in alcoholic-eosin and dehydrated using three changes of 95% EtOH and two changes of 100% EtOH for 1 min each. Finally, sections were

cleared in three changes of Xylene for 1 min each, mounted and cover slipped.

Muscle histology

The tibialis anterior (TA), soleus (SOL), extensor digitorum longus (EDL), and gastrocnemius muscles were harvested for histology. TA muscles were cut from the most distal and proximal TA tendon attachment, cleaned of extraneous tissue, blotted, and weighed. TA muscles then were stored in a 30% mixture of sucrose in PBS for 24 h, at which time, muscles were embedded in OCT (Tissue Tek), flash-frozen using dry ice and 2-methylbutane (Sigma-Aldrich), and processed for fresh-frozen histology as previously described.²⁵ TA muscles were cryosectioned at 10 μm to obtain transverse sections, and immunohistochemistry was performed for identification of laminin (extracellular matrix) and nuclei, as previously described.^{25,26} Gastrocnemius muscles were sectioned at 4 μm and fixed in 10% neutral buffered formalin and processed through paraffin, and sectioned in the University of Rochester, Center for Musculoskeletal Research Histology Core. For IHC, serial tissue sections were deparaffinized and rehydrated. Antigen retrieval was performed in citrate buffer (1x Ph6). After blocking in non-serum protein block for 60 min, sections were stained in CD45 primary antibody, overnight at 4°C. After 24 h, sections were incubated in secondary for 60 min at room temperature, then counterstained with haematoxylin. Fluorescent microscopy was performed using a Zeiss Imager: M1m microscope with AxioVision SE64 software, and representative images were used to quantify myocyte area. IHC sections were imaged using Zeiss Axioskop 40 upright microscope with SPOT RT3 camera (for brightfield/darkfield imaging only) SPOT software v4.5.9.9.

RNA isolation and reverse transcription-quantitative PCR

Muscles were flash frozen in Trizol (Ambion) at dissection and homogenized using a Bullet Blender Gold homogenizer (Next Advance BB24-AU). RNA was isolated using an RNeasy Plus Mini Kit (Qiagen) following the manufacturer's instructions. cDNA was synthesized using 500 or 1000 ng of RNA (from EDL/SOL or gastrocnemius, respectively) using qScript cDNA SuperMix (QuantaBio). Reverse transcription-quantitative PCR (RT-qPCR) was performed on a Step One Plus Real-Time PCR machine (Applied Biosystems) using PerfeCTa SYBR Green FastMix (QuantaBio). All reactions utilized the following thermal cycler conditions: 50°C for 2 min, 95°C for 2 min, 40 cycles of a two-step reaction, denaturation at 95°C for 15 s, and annealing at 60°C for 30 s. Experiments were standardized to YWAZ. Primers are provided in *Table S1*.

RNaseq data library

Total RNA concentration was determined with the NanoDrop 1000 spectrophotometer (NanoDrop), and RNA quality was assessed with the Agilent Bioanalyzer. Illumina compatible library construction was performed using the TruSeq Total

Stranded RNA Sample Preparation Kit (Illumina) following manufacturer's protocols. Briefly, rRNA was extracted from 200 ng total RNA with RiboZero magnetic beads. Residual RNA, depleted of rRNA, was chemically fragmented following the manufacturer's recommendation. First-strand cDNA synthesis was performed using random hexamer priming followed by second-strand cDNA synthesis using dUTP. End repair and 3' adenylation was performed on the double-stranded cDNA. Illumina adaptors were ligated to both ends of the cDNA, purified by gel electrophoresis and amplified with PCR primers specific to the adaptor sequences to generate amplicons of approximately 200–500 bp in size. The amplified libraries were hybridized to the Illumina single-end flow cell and amplified using the cBot (Illumina). Approximately, 40 million single-end reads of 100 nt were generated for each sample.

Serum cytokine and IGFBP-3 measurements

Pro-inflammatory cytokines IL-6 and TNF- α were measured in mice serum using a custom built Milliplex xMAP Murine Cytokine Magnetic Bead Panel (EMD Millipore) according to manufacturer's instructions. Additionally, utilizing manufacturer's protocols, serum Insulin-like Growth Factor Binding Protein-3 (IGFBP-3) levels were quantified in mice using ELISA (Abcam).

Statistical analysis

Myofibres cross-sectional area (CSA) was determined using ImageJ software. The diameter of the fibre was measured at three points along the fibre to get an average CSA. TA cell area was calculated by drawing a ROI around the extracellular space of 200 individual cells and taking the average of the sum of those cells. Results are presented as mean \pm SD. Statistical significance was determined using Independent Student's *t* tests for comparisons between two groups. One-way was used to determine fold change difference in genes of NTC and PDAC mice and two-way ANOVA was used for the comparisons of between and within group differences in (lean mass vs. time) and (lean mass vs. treatment) for NTC and PDAC groups. Kaplan–Meier estimator of survival was used to quantify survival of PDAC mice. Pearson correlation coefficient was calculated to measure the association between tumour size and survival. Independent *t* tests and one-way ANOVA were used to analyse differences between NTC and PDAC mice. A mixed-effects linear change-point regression model with a compound symmetry within-mouse correlation structure was used to estimate and compare changes in lower limb mass over time.²⁷ Analyses were performed using GraphPad Prism software (GraphPad Software, San Diego, CA, USA) version 7.2 and 8.0, R version 3.5.1, and SAS version 9.4. $P < 0.05$ was considered significant (* $P < 0.05$, ** $P < 0.01$, *** $P < 0.001$, **** $P < 0.0001$).

Results

An orthotopic murine mode of pancreatic ductal adenocarcinoma recapitulates clinical skeletal muscle wasting without tumour metastasis

To elucidate the mechanisms of PDAC-related SMW in mice, we used the *Muc1*-null PDAC model (designated KCKO) (Figure 1). Using a small animal *in vivo* Imaging System (IVIS), we verified implant tumour growth in 100% of the mice on Day 5 post injection (Figure 2A). Visualization of the bioluminescent signal [bioluminescent imaging (BLI)] confirmed KCKO tumour growth localized to the peritoneal cavity. Quantification of the BLI from Day 5 to Day 54 verified *in vivo* peri-injection tumour growth (Figure 2B and 2C). These data indicate that, while KCKO cells develop into solid tumours and advance locally, there is no distant metastasis of the tumour.

Primary tumour size is not predictive of morbidity and mortality in the murine KCKO pancreatic ductal adenocarcinoma model

To determine if tumour size correlates with morbidity and mortality in KCKO-implanted mice, we evaluated the

macroscopic and microscopic features of the primary tumour at the time of death. Post-mortem examination revealed substantial growth of the inoculated tumours at Day 40, and mice that survived to Day 60 had local spread of tumours (Figure 3A and 3B). Histological assessment showed that KCKO immortalized cell line tumours have features similar to those of human PDAC, as evidenced by formation of neoplastic glands with nuclear atypia (Figure 3C) and mucin production (Figure 3D). Interestingly, the Kaplan–Meier estimator showed a broad range of time to death post-KCKO implantation from 34 to 68 days, with a median survival time of 42 days (Figure 3E). Thus, although we found a strong positive relationship between tumour size and survival ($r^2 = 0.83$, $P < 0.0001$) (Figure 3F), these findings demonstrate that tumour volume alone does not explain survival in this model.

Longitudinal quantification of lean mass via dual-energy X-ray absorptiometry identifies onset of pancreatic ductal adenocarcinoma-related muscle wasting

Lean mass of murine PDAC mice were longitudinally assessed via DEXA imaging (Figure 4A). Post-mortem analysis of total body weight (TBW) with and without the tumour burden

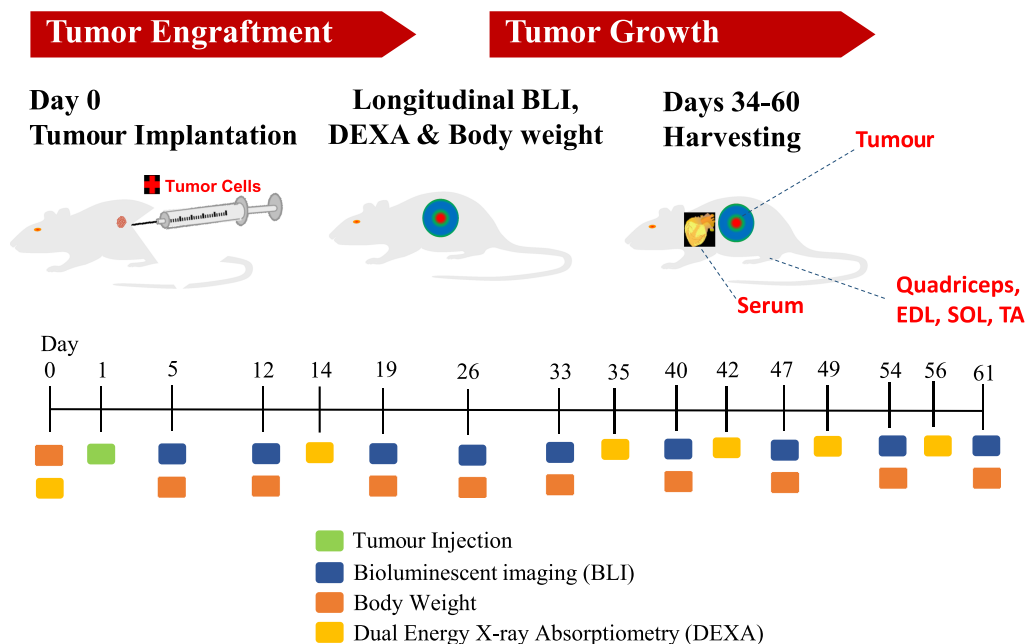


Figure 1 Schematic overview of the murine pancreatic ductal adenocarcinoma (PDAC) skeletal muscle wasting model. Seven-week-old female C57/B6 mice ($n = 19$) were anaesthetized for laparotomy and received orthotopic injections of 2×10^5 KCKO-Luc tumour cells in 0.1 mL of saline in their pancreas. *In vivo* BLI was performed on Day 5 to verify tumour engraftment, and tumour bearing mice were maintained in standard isolation cages with 12 h light:dark cycle, and given ad libitum access to water and standard chow. Longitudinal assessments of tumour growth (BLI), body mass (DEXA) and weight were obtained on the indicated days. Mice were sacrificed when they reached end stage disease, as defined by the IACUC's definition of 'failure to thrive'. Following euthanasia, skeletal muscles [quadriceps, extensor digitorum longus (EDL), soleus (SOL), and tibialis anterior (TA)] and pancreatic ductal adenocarcinoma (PDAC) tumours were harvested for histology, and cardiac puncture was performed to obtain serum for Luminex assay. A separate cohort of 7 week-old female C57/B6 mice ($n = 10$) that did not receive any treatments was used as no tumour controls (NTCs).

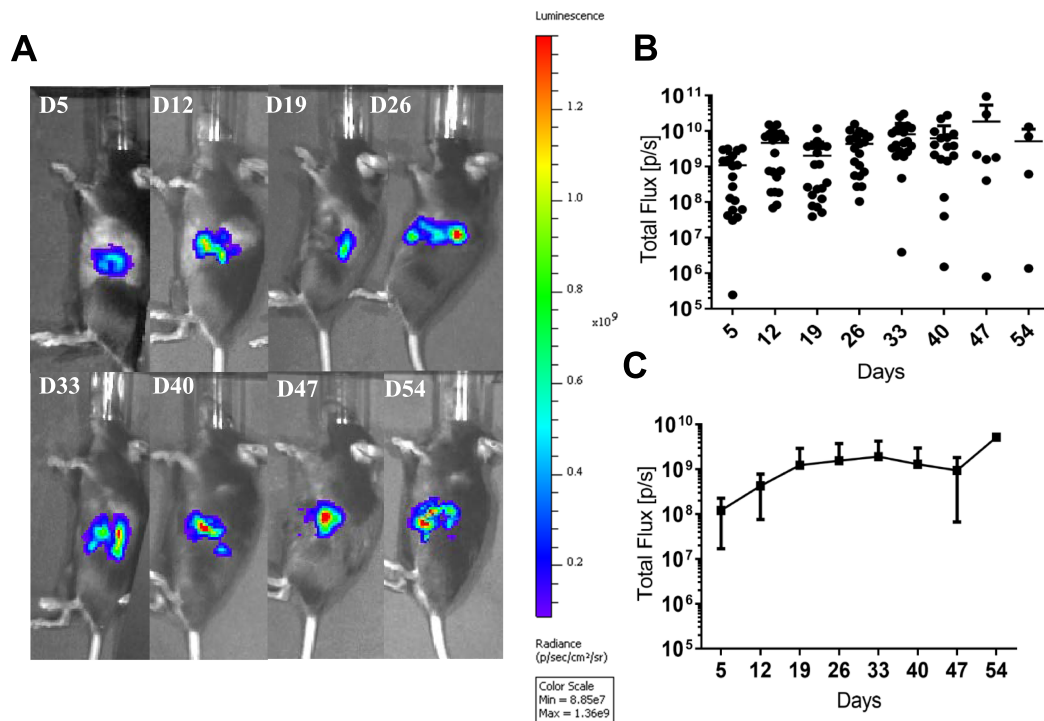


Figure 2 Longitudinal bioluminescent imaging (BLI) demonstrates stable *in vivo* pancreatic ductal adenocarcinoma (PDAC) growth localized to the retroperitoneal cavity over 54 days of syngeneic PDAC engraftment. The mice described in Figure 1 were subjected to *in vivo* BLI as described in Materials and Methods, and the (A) relative signal intensity of the engrafted tumour in a representative mouse that was studied out to Day 54 is shown. Note that the longitudinal BLI signal radiating from the mouse's pancreas is fairly consistent throughout the study period and there was no detectable BLI signal outside of this abdominal region. (B) The BLI signal for each mouse in the study is presented with the mean \pm SD on the day of assessment. (C) Longitudinal BLI values for mice that survived throughout the entire assessment period ($n = 4$) are presented with the mean \pm SD. No statistical differences in BLI signal intensity between any of the time points of this subgroup were noted.

showed a significant decrease in TBW after resection of the tumour ($P < 0.0001$) (Figure 4B). TBW and lean mass of both PDAC and NTC mice were measured at set time intervals. A significant decrease in lean mass was observed at Day 38, and this was sustained through Day 56; in contrast, no difference was observed in TBW between the groups during this period (Figure 4C and 4D), as loss in lean body mass was offset by increased tumour mass. Rates of change in lower limb mass over time were estimated and tested within a mixed-effects linear change-point regression model.²⁷ This model included random effects in mice to account for the repeated measures over time by assuming a compound symmetry within-mouse correlation structure. The estimated change point was obtained from the model, and slopes before and after the change-point were estimated and compared. The mixed-effects linear change-point regression model for lower limb mass revealed an estimated change-point at Day 38.6 (95% confidence interval: 33.2–44.1). There was an increase over the initial 38.6 days (slope = 0.0003 g/day, standard error = 0.0001, $P = 0.007$), followed by a decrease after day 38.6 (slope = -0.002 g/day, standard error = 0.0003, $P < 0.0001$); the difference in slopes was substantial ($P < 0.0001$). Thus, using longitudinal assessment of lean mass with DEXA, we were able to detect the onset of SMW, which is

crucial for intervention studies and may aid in identifying stage and progression of disease in patients with PDAC.

Histological evidence of skeletal muscle wasting in mice with end-stage pancreatic ductal adenocarcinoma

Ex vivo analysis of the EDL, SOL, and TA muscles from mice with end-stage PDAC showed a significant decrease in CSA when compared with NTC (Figure 5A, 5B, and 5C). TA mass was significantly decreased in PDAC mice (Figure 5D). These data confirm our *in vivo* findings of PDAC-related SMW in this murine PDAC model.

Increased immune cell infiltration and elevated pro-inflammatory cytokine levels in skeletal muscle of mice with end-stage pancreatic ductal adenocarcinoma experiencing skeletal muscle wasting

To elucidate the cellular and molecular mechanisms responsible for SMW in KCKO-bearing mice, we completed a

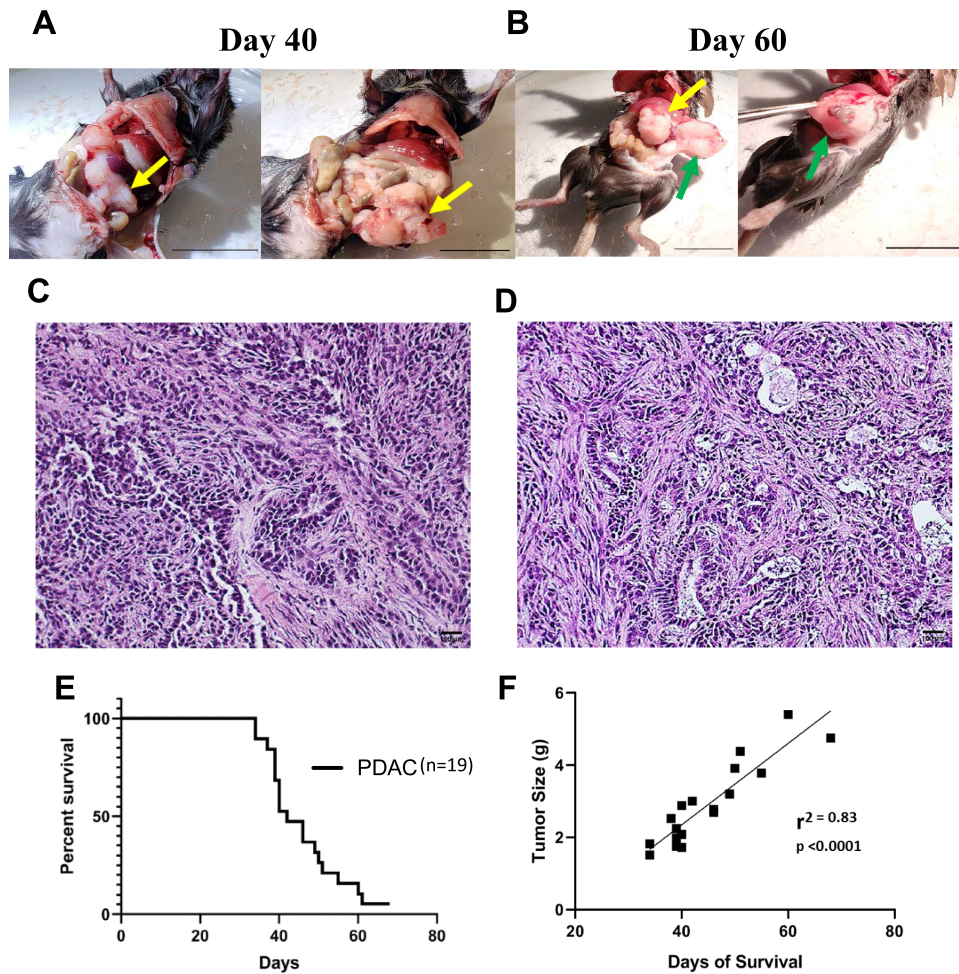


Figure 3 Tumour burden and survival are positively correlated in this murine pancreatic ductal adenocarcinoma (PDAC) model. Gross images of PDAC in mice that achieved failure to thrive on Day 40 (A) and Day 60 (B), post-inoculation are presented to illustrate the primary tumour (yellow arrows) and local metastases (green arrows). The $\times 10$ micrographs of representative haematoxylin and eosin stained sections of primary PDAC tumours are presented to illustrate their histopathology including: ductal adenocarcinoma with well-differentiated glands and marked nuclear atypia infiltrating the stroma (C), and mucinous ductal adenocarcinoma surrounded by malignant epithelium (D). (E) The Kaplan–Meier estimator of survival of the PDAC tumour bearing mice is shown ($n = 19$). The onset of failure to thrive in this cohort ranged between 30 and 60 days post-inoculation. (F) A linear regression analysis is presented to illustrate the strong correlation between survival (days) and tumour wet weight (G) at the time of failure to thrive ($r^2 = 0.83$; $P < 0.0001$).

series of histological and gene expression studies on skeletal muscle tissue. Mice with end-stage PDAC had increased intramuscular immune cell infiltration (Figure S1), which was confirmed by CD45⁺ staining (Figure 6A and 6B). Real-time qPCR analysis revealed a significant increase in mRNA expression levels of pro-inflammatory cytokines, *il-1 α* , *il-1 β* , *il-6*, and *tnfa*, in the quadriceps muscle of PDAC mice with terminal disease (Figure 6C). In addition, serum IL-6 and TNF- α levels were up-regulated in these animals (Figures 6D and 6E). Consistent with prior studies and established paradigm, these findings underscore local and systemic inflammation as key factors in the pathogenesis of PDAC-related SMW.

IGFBP-3 dysregulation in multiple functional genomic pathways during pancreatic ductal adenocarcinoma-associated muscle wasting

We completed a non-hypothesis-driven differential gene expression study of PDAC muscle vs. NTC. Bulk RNA sequencing was used to identify expressed genes associated with the phenotype of PDAC-related SMW. Among the differentially expressed genes, mRNA levels of 1296 genes were up-regulated, and 1453 genes were down-regulated using a threshold of a 1.5-fold change and FDR of < 0.001 (S2A). Of these differentially expressed genes, an ingenuity pathway

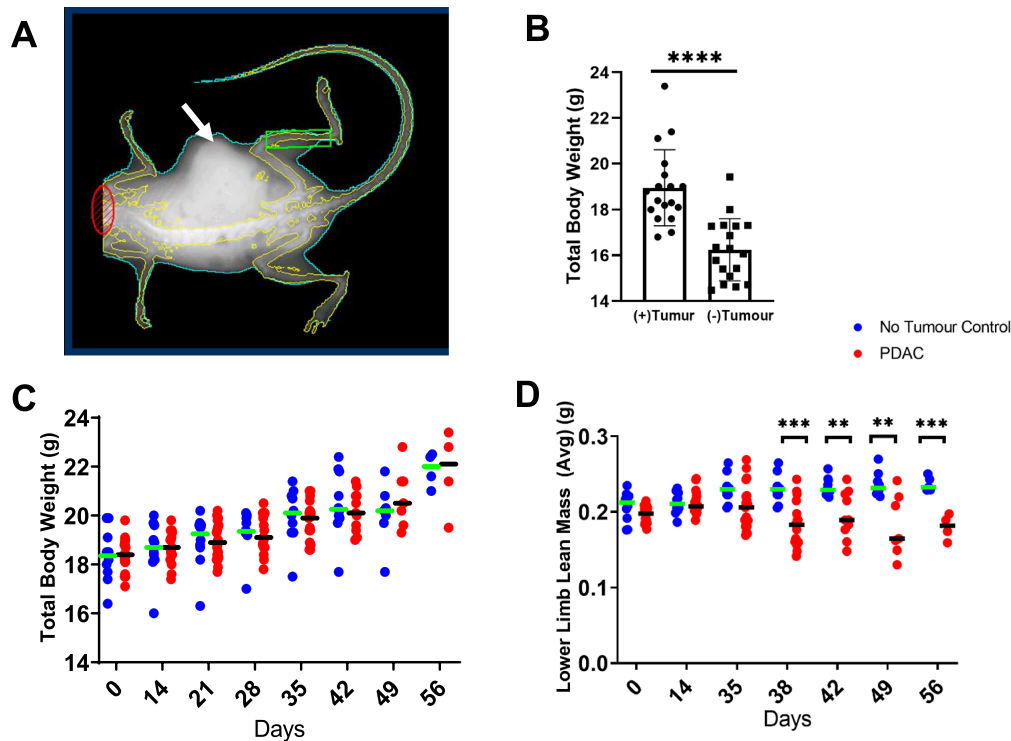


Figure 4 Longitudinal quantification of lean mass via DEXA demonstrates commencement of pancreatic ductal adenocarcinoma (PDAC)-related muscle wasting within 38 days of tumour implantation, which cannot be detected by assessment of total body weight. Mice were randomized to two groups prior to orthotopic tumour injections: (1) PDAC tumour bearing; ($n = 19$) and (2) non-tumour control (NTC); ($n = 10$). Longitudinal dual-energy X-ray absorptiometry (DEXA) and total body weight measurements were performed as described in Materials and Methods. (A) A representative DEXA scan image of a PDAC mouse is shown to illustrate segmentation of the head (red oval), body (green outline), the primary tumour mass (arrow), and the region of interest for lean mass analysis (box over lower leg). (B) The total body weight (TBW) of the PDAC-bearing mice was determined prior to tissue harvest, and the data are presented as TBW (+ tumour) and net weight (– tumour) after primary tumour harvest for each mouse with the mean \pm SD ($****P < 0.0001$). (C) The cross-sectional TBW for all mice in the study are presented with the mean of the group for Days 0, 14, 21, and 35. For the later time points, TBW is presented for each mouse that is alive at that time point. No differences between groups were observed. (D) The cross-sectional lower limb mass determined by DEXA of all mice in the study are presented with the mean of the group for Days 0, 14, and 35. For the later time points, lower limb mass is presented for each mouse alive at that time point ($**P < 0.01$, $***P < 0.001$, $****P < 0.0001$).

analysis of upstream regulators indicated the predicted dysregulation of 50 pathways (Table S2). Next we assessed gene changes within the top altered upstream regulator growth pathways. Thus, angiotensinogen, IGF-1, myostatin, TGF β , and VEGF were selected for further analysis (Figure 7A). A Venn diagram analysis of altered genes within these pathways revealed Insulin-like Growth Factor Binding Protein-3 (IGFBP-3) to be the sole common nodal point (Figure 7B). ELISA confirmed that serum IGFBP-3 levels are higher in mice with PDAC than NTC mice (Figure 7C). Additionally, qPCR analysis confirmed up-regulation of *igfbp-3*, associated with concomitant increases in levels of the adipogenic genes, *c/ebpa*, β , and Δ , along with *ppary* and *fabp4* (Figure 7D). Intriguingly, we found *igfbp-3* mRNA to be differentially expressed in the muscle of PDAC mice with SMW compared with PDAC mice without wasting (Figure 7E). These data suggest that adipogenesis is induced during end-stage

PDAC-related SMW and that IGFBP-3 may be a potential mediator of adipogenesis.

Intramuscular adipose deposits in quadriceps muscle of mice with pancreatic ductal adenocarcinoma-associated muscle wasting

To investigate the relationship between increases in IGFBP-3 and genes associated with adipogenesis, we performed Oil Red-O staining on skeletal muscle samples from NTC and mice with PDAC-associated SMW. We observed numerous fat droplets in muscle fibres in PDAC mice, but very few in NTC mice (Figure 8A–8D) and confirmed this quantitatively in digital slides using a Visiopharm image analysis system (Figure 8E–8H). This novel finding implicates an increase in

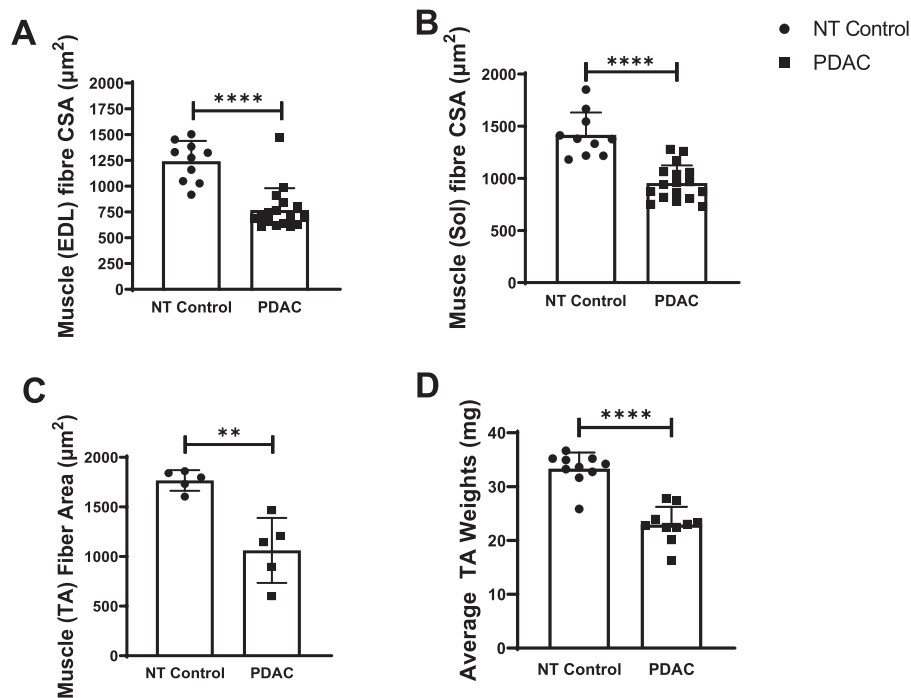


Figure 5 Quantitative analysis of skeletal muscle atrophy in terminal mice with pancreatic ductal adenocarcinoma (PDAC). Following euthanasia due to failure to thrive, the extensor digitorum longus (EDL) and soleus (SOL) muscles were harvested from PDAC ($n = 19$) bearing and non-tumour (NT) control (NTC) ($n = 10$) mice, and stained with DAPI for calculation of CSA (100 fibres per mouse). Tibialis anterior (TA) muscles were dissected and weighed. After which, TA muscles were frozen and stained with Laminin for measurement of cross-sectional area (CSA). Quantification of (A) EDL and (B) SOL muscle fibres at the time of sacrifice from NT and PDAC-bearing mice are presented, along with quantification of (C) TA CSA (μm^2) ($n = 5$) and (D) weights (mg) ($n = 10$) with the mean \pm SD (** $P < 0.01$) (**** $P < 0.0001$).

myocellular lipid concentration as a factor in the development and/or progression of PDAC-related SMW.

Discussion

Pancreatic cancer is a highly lethal treatment refractory disease that is associated with severe SMW.²⁸ SMW is prognostic of treatment failure, poor surgical outcomes, and a shorter time to tumour progression related to survival.^{6,29–31} However, the mechanisms that lead to SMW in patients with PDAC remain unclear. In this study, we established the first model of PDAC-related SMW using a Muc 1-null model (KCKO). In addition, we confirmed the recently described increase in striated muscle immune cell infiltration in PDAC¹⁶ and discovered a novel triad of SMW involving pathologic fat accumulation in myocytes, IGFBP-3, and inflammation, associated with dysregulation of pathways of protein synthesis. Using *in vivo* DEXA, longitudinal analysis of lean mass in KCKO tumour-bearing mice, we identified the onset of SMW around day 38 post tumour cell inoculation. In addition to marking the onset of SMW in this model, it is also important to note the lack of significant decrease in lean muscle mass after Day 38. Remarkably, this onset of muscle wasting seems

to also mirror the time in which animals begin to succumb to disease in this model. Clinically, refractory cachexia is defined as the end stage of disease and the point in which muscle wasting cannot be reversed as death is imminent.³² Future studies on cancer-related muscle wasting in this KCKO model should capitalize on the use of DEXA to longitudinally assess lean mass to determine if a molecular marker such as IGFBP-3 can be used indiscriminately to signal the onset on SMW. This finding will facilitate prospective research and future intervention studies to prevent and treat SMW in this model. *Ex vivo* analysis confirmed SMW in the lower limbs of mice with terminal PDAC. Furthermore, we determined that increased muscle immune cell infiltration and fat accumulation, and IGFBP-3 serum levels are associated with PDAC-related SMW. Taken together, this is the first study to establish SMW in a KCKO murine model of PDAC, and to show histologic evidence of increased fat accumulation in the muscle cells of mice with PDAC-related SMW.

Research supports the immunosuppressive role of myeloid cells in the development of PDAC tumours and growth through neutralization of cytotoxic T cells.^{16,17} Furthermore, these cells are responsible for the systemic and local up-regulation of pro-inflammatory cytokines, such as TNF- α , IL-1, and IL-6,¹⁶ that cause muscle catabolism.^{11,14} To examine pathogenesis of PDAC-related SMW in KCKO bearing

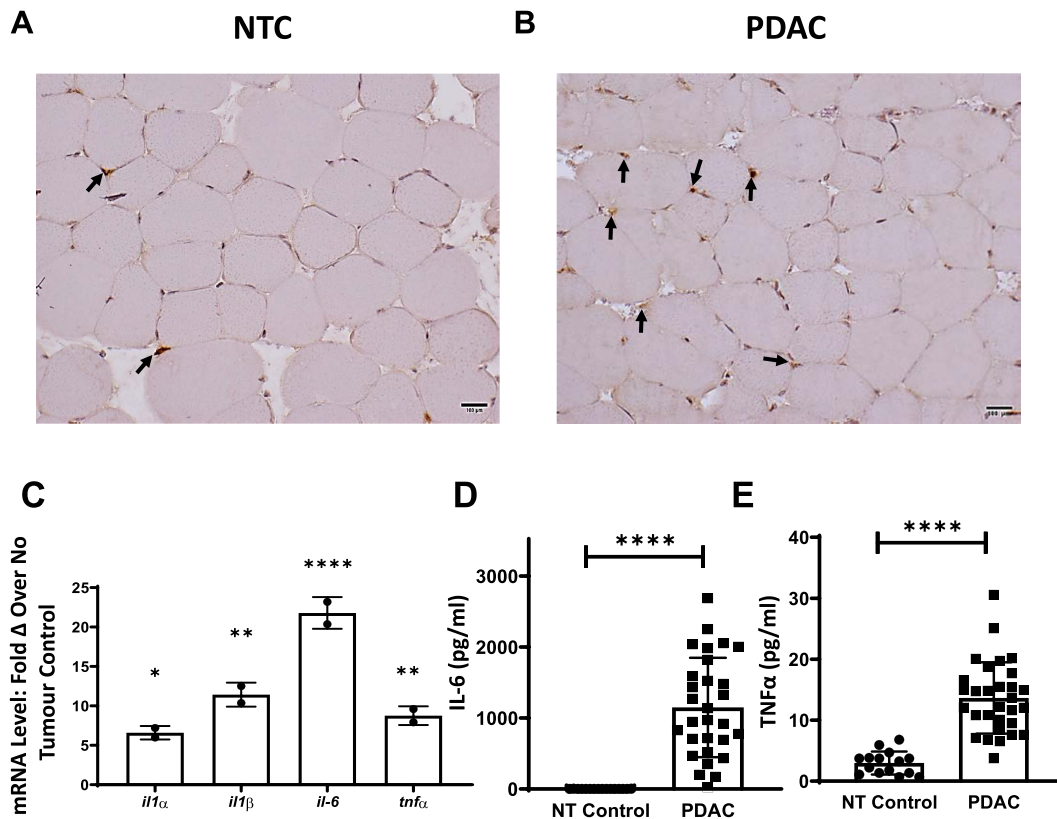


Figure 6 Confirmation of increased CD45+ cell infiltration and elevated pro-inflammatory cytokine in the muscle of mice experiencing pancreatic ductal adenocarcinoma (PDAC)-related skeletal muscle wasting (SMW). Gastrocnemius muscles of non-tumour control (NTC) and PDAC mice were dissected as described in Figure 1, and immunohistochemistry was performed with labelled antibodies against CD45. Representative $\times 40$ photomicrographs of the immunostained muscles are shown to illustrate the numbers of CD45+ cells (black arrows) within muscle from (A) NTC and (B) PDAC mice. (C) Real-time reverse transcription-quantitative PCR (RT-qPCR) of total RNA of quadriceps muscle tissue from PDAC ($n = 5$) and NTC ($n = 5$) mice was performed to assess pro-inflammatory gene expression, and the data are presented as the mean fold change over NTC \pm SD. Gene expression studies were performed by pooling total RNA from five mice per group, and each group was analysed in duplicate. Serum levels of (D) IL-6 and (E) TNF from NTC and PDAC mice were determined by Luminex, and the data for each mouse with the mean \pm SD of the group are shown. (* $P < 0.05$; ** $P < 0.01$; *** $P < 0.001$; **** $P < 0.0001$).

mice, we completed a series of histological and gene expression studies on skeletal muscle tissue. Our findings are consistent with other reports documenting an increase in immune cell infiltration and up-regulation of pro-inflammatory cytokines in the muscles of animal models and in patients with cancer cachexia.^{11,16} To better understand the cellular and molecular mechanisms that mediate SMW in our model, we performed a differential bulk RNAseq analysis of NTC vs. PDAC mice. We observed the predicted significant increases in macrophage and pro-inflammatory gene expression and a surprising increase in adipogenic and *igfbp3* mRNA levels in skeletal muscle from PDAC mice. This discovery of macrophage and adipogenic gene expression in wasting muscle tissue has a molecular basis. In addition to their known role in adipogenesis, CCAAT/enhancer-binding proteins (C/EBP) play an important role in the regulation of cell proliferation and differentiation and are induced in terminally differentiating macrophages.³³ Furthermore, the up-regulation of genes that

regulate both adipogenesis and macrophage differentiation are consistent with increases in IGFBP-3.

Canonical insulin-like growth factor binding proteins (IGFBPs) bind insulin-like growth factors (IGFs) to stabilize the ligand complex, and enhance the half-life and bio-distribution of IGFs to target tissues.³⁴ IGFBP-3, a major IGFBP species in circulation, binds 75% to 90% of circulating IGF-1.²² This function of IGFBP-3 is vital to muscle homeostasis given the major role that IGF-1 plays in protein synthesis. However, excessive increases in IGFBP-3 that are not accompanied by increases in IGF-1 result in suppressed IGF-1 stimulated myoblast proliferation, perturbed protein synthesis, and apoptosis.^{34,35} Previous research suggest that the role IGFbps play in cellular proliferation and differentiation are IGF dependent; however, recent studies completed on fibroblasts and human epithelial cells support an IGF-independent role of IGFBP-3 on cell growth, proliferation, and survival.²² Thus, more research is needed to elucidate

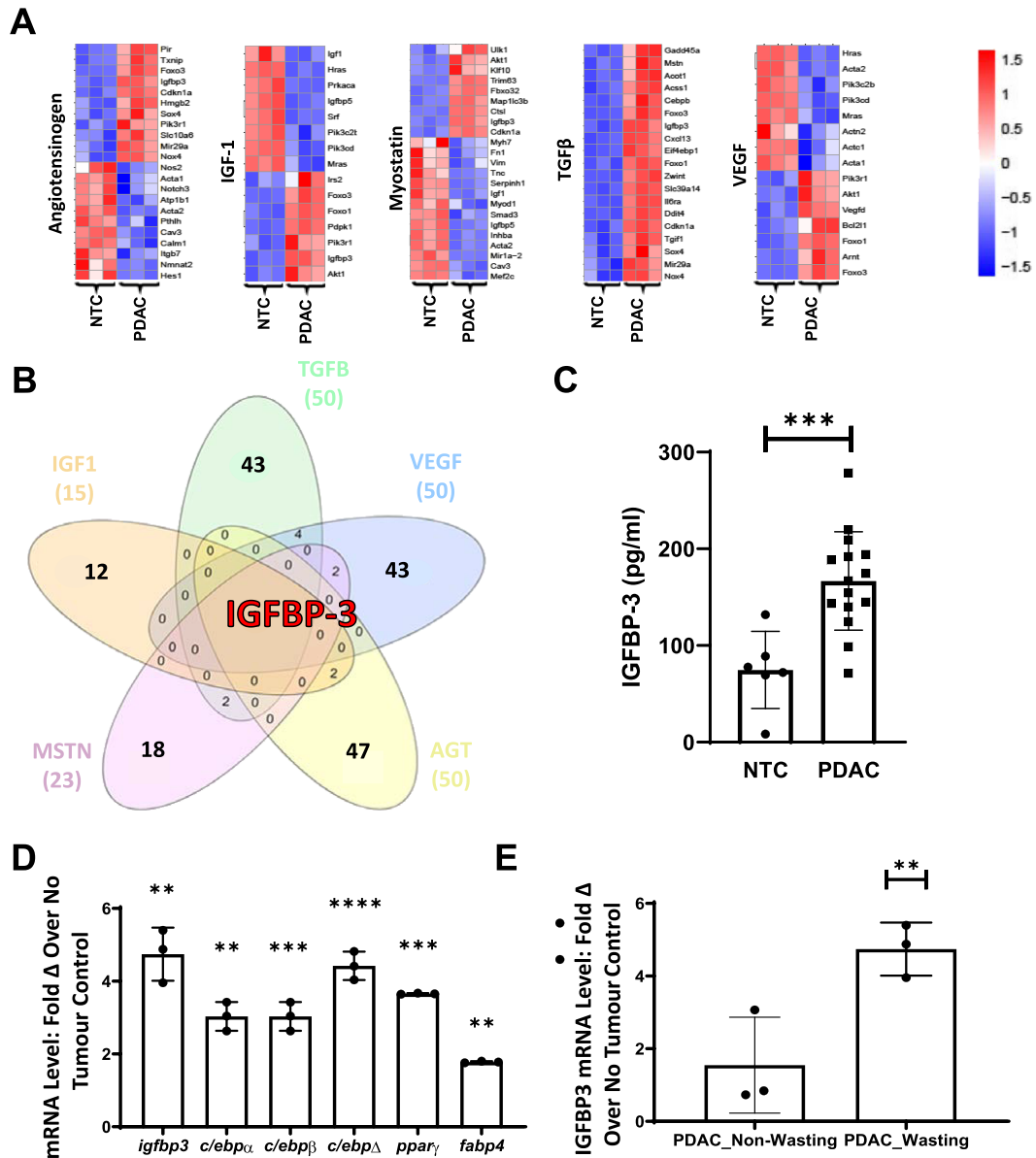


Figure 7 Bulk RNAseq reveals IGFBP-3 dysregulation in multiple functional genomic pathways during pancreatic ductal adenocarcinoma (PDAC)-associated muscle wasting. (A) Bulk RNAseq was performed on quadriceps muscles from non-tumour control (NTC) and PDAC-bearing mice ($n = 3$), and heat maps of the differentially expressed genes in the indicated pathways are shown to illustrate the high (red) vs. and low (blue) mRNA levels in the pathway. (B) Venn diagram analysis reveals *IGFBP-3* as the lone gene that is dysregulated in all the functional genomic pathways. (C) IGFBP-3 levels in serum from NTC and PDAC-bearing mice were determined by ELISA, and the data for each mouse with the mean \pm SD of the group are shown. (D) Real-time reverse transcription quantitative PCR (RT-qPCR) of total RNA of quadriceps muscle tissue from the mice was performed to assess *igfbp3* and macrophage marker gene expression, and the data are presented as the mean fold change over NTC \pm SD. Gene expression studies were performed by pooling total RNA from five mice per group, and each group was analysed in triplicate. Post hoc analysis of the *igfbp3* mRNA levels determined in (D) was performed to illustrate the four-fold increase in quadriceps muscles of PDAC mice with wasting ($n = 4$) vs. without wasting ($n = 3$) determined dual-energy X-ray absorptiometry (DEXA) (** $P < 0.01$; $P < 0.001$; **** $P < 0.0001$).

the underlying molecular mechanisms involved in these biological actions of IGFBP-3.

IGFBP-3 is up-regulated both locally^{36–38} and systemically³⁹ in patients with pancreatic cancer and is associated with a poor prognosis.^{37,38} Overexpression of IGFBP-3 by muscle-associated macrophages has been implicated in

increased ubiquitination-associated proteolysis, inhibition of myogenesis, and PDAC-associated SMW.^{36,40–43} In support of these findings, our RNAseq analyses revealed dysregulation of the protein ubiquitin and MYOD1 pathways (Figure S1). We also found dysregulation of the insulin-like growth factor-1 (IGF-1), myostatin (MSTN), transforming

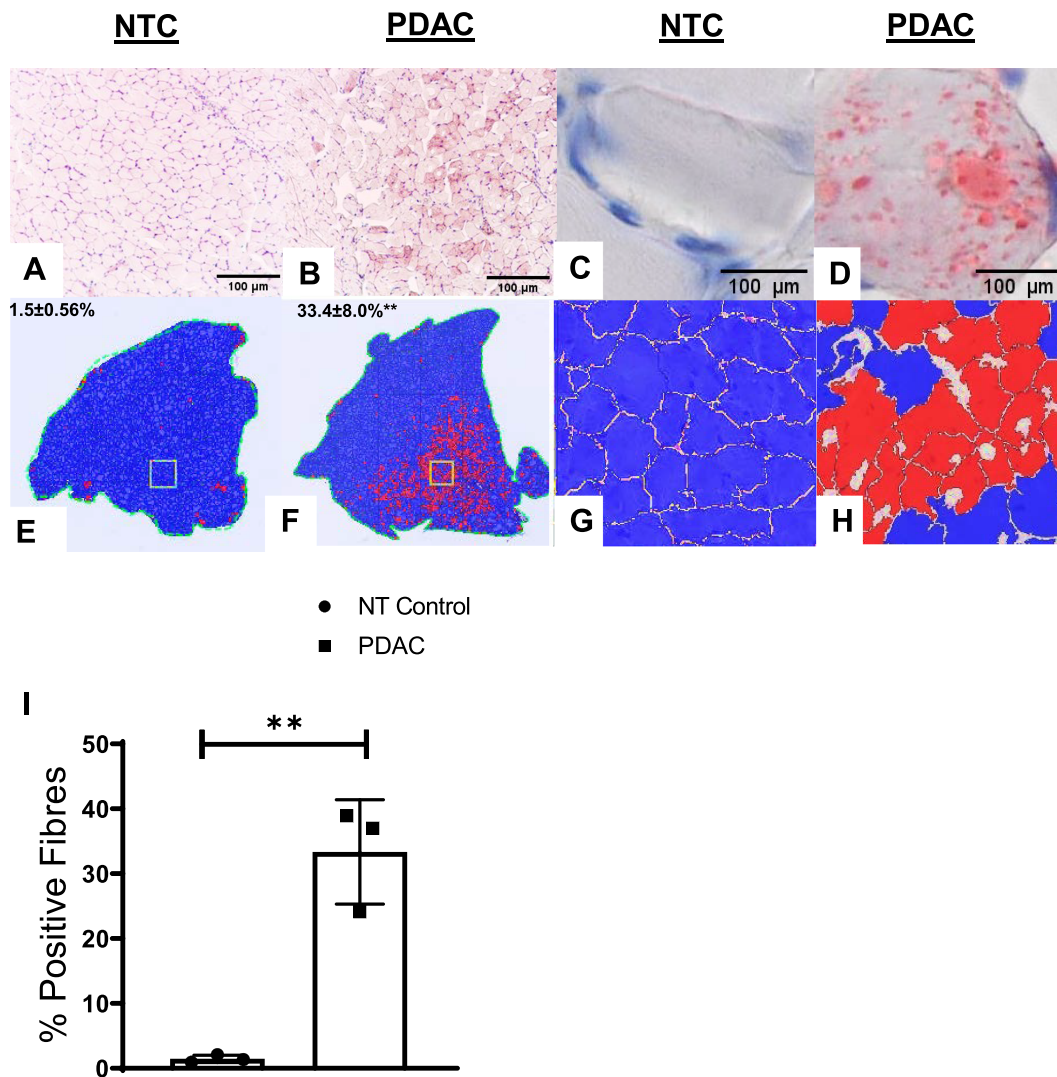


Figure 8 Intramuscular adipose deposits in quadriceps muscle of mice with pancreatic ductal adenocarcinoma (PDAC) associated muscle wasting. The tibialis anterior (TA) muscles from non-tumour control (NTC) (A–D) and mice with PDAC-associated muscle wasting (E–H) described in Figure 5 were flash frozen and processed for Oil Red-O-stained histology, and representative images are shown at $\times 10$ (A,E), and $\times 40$ (B,F) to illustrate the prevalence of adipogenesis in the muscle fibres and the fat lobules in the fibres, respectively. To quantify the number of Oil Red-O positive fibres per section via computer automated histomorphometry, we wrote an app in Visiopharm that imports the digital histology images, segments the individual fibres, and this binarizes positive and negative fibres based on the intensity of the red staining to produce the number of fibres and per cent of positive (C,D,G,H). (I) PDAC muscles had a significantly greater per cent of positive fibres $P = 0.002$ compared with NTC. Data are presented as (% positive fibres) mean \pm SD.

growth factor- β (TGF β), vascular endothelium growth factor (VEGF), and angiotensinogen (AGT) pathways (Table S2). In light of their known role in muscle homeostasis,¹¹ we used an ingenuity pathway analysis of upstream regulators to identify all genes associated with these pathways. A Venn diagram analysis of the genes associated with these five dysregulated pathways identified *IGFBP-3* as the only gene common to all of them.

Recently, it was demonstrated that pancreatic cells induce muscle wasting via IGFBP-3 production *in vitro*.³⁶ Furthermore, IGFBP-3 secreted either by tumour cells or

macrophages has been implicated in PDAC-related SMW. IGFBP-3 expression increases transiently in skeletal muscle during repair and after injury, and these changes occur in muscle-associated macrophages.⁴³ Although IGFBP-3 has been shown to inhibit differentiation of pre-adipocytes under physiological conditions, pathological increases of IGFBP-3 stimulate brown adipocyte differentiation.³⁴ Our qPCR analysis confirmed the up-regulation of *igfbp-3* mRNA expression in the quadriceps muscles of mice with advanced PDAC. We also determined that IGFBP-3 is significantly increased in the serum of these animals. Interestingly, *igfbp-3* was

differentially expressed in the muscle of PDAC mice with wasting compared with PDAC mice without wasting. These findings suggest that up-regulation of IGFBP-3 may be a key factor in the initiation of SMW in this model. In support of this, Judge *et al.* found that skeletal muscle taken from patients experiencing the severest cachexia had significantly higher amounts of IGFBP-3, macrophage infiltration, and lipid deposition compared with non-cachectic and non-cancer controls.⁴⁴ Thus, more research is needed to understand the relationships among increases in IGFBP-3, macrophage infiltration, adipogenesis, and PDAC-related SMW.

To further investigate the relationship between increases in IGFBP-3 and genes associated with adipogenesis, we performed Oil Red-O staining on skeletal muscle samples from NTC and mice with PDAC-associated SMW and developed an automated Visiopharm image analysis algorithm to quantify fat accumulation in myocytes. Using this algorithm, we found that PDAC mice had more than a 30-fold increase in positively stained muscle fibres when compared with NTC, which further validates our RNAseq results. Of note is that this intracellular lipid accumulation is distinct from the canonical intermuscular adipose tissue observed in older adults and across a wide variety of comorbid conditions, such as stroke, spinal cord injury, diabetes, and chronic obstructive pulmonary disease.⁴⁵ Thus, this may represent a unique pathology, the effects of which remain unknown at this time. Thus, future research should investigate the relationships among up-regulated adipogenesis, the onset of SMW, and death from PDAC.

In conclusion, the results of this study support the role of increased systemic and local pro-inflammatory cytokines in cancer-related SMW. We also show dysregulation in pathways associated with anabolism. To our knowledge, this is the first study to histologically confirm myocyte fat accumulation in a murine PDAC model and show that this increase in adiposity is associated with increased immune cell infiltration and IGFBP-3 expression. However, our study has notable limitations. First, we did not study natural death from PDAC. Rather, we followed our IACUC's definition of 'failure to thrive' as an endpoint for euthanasia of mice with advanced stage PDAC, which may have biased our survival analysis. However, the criteria for failure to thrive have been validated previously as a survival endpoint,⁴⁶ and were applied consistently across all animal groups. Furthermore, animals were sacrificed on the advice of university veterinarians without knowledge of their treatment. With animal welfare justification from this study, future IACUC-approved studies using death as an endpoint can be performed to confirm our findings and investigate this as an independent outcome variable. Second, we did not sacrifice animals at set time intervals to better characterize the association of increased myocyte adiposity and SMW. Further research should investigate this relationship and the relationship

between increased inflammation and the dysregulated pathways identified in our gene expression studies. Lastly, we did not determine the cellular source of the increased IGFBP-3. Of note is that other studies have investigated this and found that both pancreatic tumour cells and macrophages secrete IGFBP-3.^{36,43} Gain and loss of function experiments are also needed to establish the role of IGFBP-3 in this murine model of PDAC. Although this research does have some limitations, the findings of increased myocyte adiposity and IGFBP-3 are both novel and exciting. However, more research is needed to elucidate mechanisms that lead to these pathologies and determine their relationship with PDAC-related SMW. Importantly, our ability to identify the onset of SMW in this murine model of PDAC is especially significant, as its clinical translation is vital to better understanding SMW and identifying the appropriate timing of therapeutic intervention in patients with PDAC.

Acknowledgements

This work was supported by grants from National Institutes of Health, R01 CA168863 (0610320003), SP0RE P50 CA196510, 1S10RR027340, and P30 AR069655. We thank the members of the Histology, Biochemistry & Molecular Imaging Core and the Biomechanics, Biomaterials, and Multimodal Tissue Imaging Core in the Center for Musculoskeletal Research.

Online supplementary material

Additional supporting information may be found online in the Supporting Information section at the end of the article.

Figure S1. Increased inflammatory cell infiltration in skeletal muscle of mice with end-stage PDAC experiencing muscle wasting. TA muscles were harvested from NTC ($n = 15$) and PDAC ($n = 30$) mice and processed for H&E stained histology. Representative 10x photomicrographs with magnified images (inset) are shown (A,B), with quantification of nuclei per 500 μm^2 field, and the data are presented as mean of 5 fields \pm std. Note the normal myonuclei and satellite cells (white arrows), and nuclei of infiltrating inflammatory cells (blue arrows). Data for each mouse with the mean \pm SD of the group are shown. (***) $p < 0.001$

Figure S2. Dysregulation of adipogenic, inflammatory, and growth factor pathways in skeletal muscle of mice with terminal PDAC. Bulk RNA sequencing of total RNA from mice quadriceps muscle tissue described in Figure 1 was performed to assess (A) Differentially Expressed Genes, (B) adipogenic, (C) pro-inflammatory, and (D) growth factor gene

expression in the quadriceps muscle of mice experiencing PDAC-related SMW. Heat maps of the gene expression were generated as described in Figure 7, and illustrate the relative increase (red) or decrease (blue) in mRNA levels

Table S1. qPCR primer list

Table S2. Upstream Regulator Genes

Conflict of interest

Calvin L. Cole, John Bachman, Joseph Murphy, Jian Ye, Scott Gerber, Christopher Beck, Brendan Boyce, Joe Chakkalakal, Gowrishankar Muthukrishnan, Edward Schwarz, and David Linehan have no conflict of interest.

References

- Cruz-Jentoft AJ, Bahat G, Bauer J, Boirie Y, Bruyère O, Cederholm T, et al. Sarcopenia: revised European consensus on definition and diagnosis," (in eng). *Age Ageing* 2019;**48**:601.
- Ninomiya G, Fujii T, Yamada S, Yabusaki N, Takami H, Kanda M, et al. Clinical impact of sarcopenia on prognosis in pancreatic cancer. *Pancreatology* 16:S91.
- Peng P, Hyder O, Firoozmand A, Kneuert P, Schulick RD, Huang D, et al. Impact of sarcopenia on outcomes following resection of pancreatic adenocarcinoma. *J Gastrointest Surg* 2012;**16**:1478–1486.
- Takagi K, Yagi T, Yoshida R, Umeda Y, Nobuoka D, Kuise T, et al. Sarcopenia predicts postoperative infection in patients undergoing hepato-biliary-pancreatic surgery. *Int J Surg Open* 2017;**6**:12–18.
- Huang DD, Wang SL, Zhuang CL, Zheng BS, Lu JX, Chen FF, et al. Sarcopenia, as defined by low muscle mass, strength and physical performance, predicts complications after surgery for colorectal cancer," (in eng). *Colorectal Dis* 2015;**17**:O256–O264.
- Wang SL, Zhuang CL, Huang DD, Pang WY, Lou N, Chen FF, et al. Sarcopenia adversely impacts postoperative clinical outcomes following gastrectomy in patients with gastric cancer: a prospective study. *Ann Surg Oncol* 2016;**23**:556–564.
- Siegel RL, Miller KD, Jemal A. Cancer statistics, 2020. *CA Cancer J Clin* 2020;**70**:7–30.
- Henderson SE, Makhijani N, Mace TA. Pancreatic cancer-induced cachexia and relevant mouse models. *Pancreas* 2018;**47**:937–945.
- Aversa Z, Costelli P, Muscaritoli M. Cancer-induced muscle wasting: latest findings in prevention and treatment. *Ther Adv Med Oncol* 2017;**9**:369–382.
- Amundson JR, Williams JK, Benjamin AJ, Witmer HDD, Roggin KK. The impact of sarcopenia on patients undergoing treatment for pancreatic ductal adenocarcinoma. *J Pancreatol* 2020;**3**:59–71.
- Cole C, Kleckner I, Jatoi A, Schwarz E, Dunne R. The role of systemic inflammation in cancer-associated muscle wasting and rationale for exercise as a therapeutic intervention. *J Cachexia Sarcopenia Muscle Rev* 2018;**3**:19.
- Costamagna D, Costelli P, Sampaolesi M, Penna F. Role of inflammation in muscle homeostasis and myogenesis. *Mediators Inflamm* 2015;**2015**:805172.
- Babic A, Schnure N, Neupane NP, Zaman MM, Rifai N, Welch MW, et al. Plasma inflammatory cytokines and survival of pancreatic cancer patients. *Clin Transl Gastroenterol* 2018;**9**:145–145.
- Padoan A, Plebani M, Basso D. Inflammation and pancreatic cancer: focus on metabolism, cytokines, and immunity. *Int J Mol Sci* 2019;**20**:676.
- Shadhu K, Xi C. Inflammation and pancreatic cancer: an updated review. *Saudi J Gastroenterol* 2019;**25**:3–13.
- Shukla SK, Markov SD, Attri KS, Vernucci E, King RJ, Dasgupta A, et al. Macrophages potentiate STAT3 signaling in skeletal muscles and regulate pancreatic cancer cachexia. *Cancer Lett* 2020;**484**:29–39.
- Mills BN, Connolly KA, Ye J, Murphy JD, Uccello TP, Han BJ, et al. Stereotactic body radiation and interleukin-12 combination therapy eradicates pancreatic tumors by repolarizing the immune microenvironment. *Cell Rep* 2019;**29**:406–421.e5.
- Besmer DM, Curry JM, Roy LD, Tinder TL, Sahraei M, Schettini J, et al. Pancreatic ductal adenocarcinoma mice lacking mucin 1 have a profound defect in tumor growth and metastasis. *Cancer Res* 2011;**71**:4432–4442.
- Han BJ, Murphy JD, Qin S, Ye J, Uccello TP, Garrett-Larsen J, et al. Microspheres encapsulating immunotherapy agents target the tumor-draining lymph node in pancreatic ductal adenocarcinoma. *Immunol Invest* 2020;**49**:808–823.
- Mulder SE, Dasgupta A, King RJ, Abrego J, Attri KS, Murthy D, et al. JNK signaling contributes to skeletal muscle wasting and protein turnover in pancreatic cancer cachexia. *Cancer Lett* 2020;**491**:70–77.
- Talbert EE, Cuitiño MC, Ladner KJ, Rajasekera PV, Siebert M, Shakya R, et al. Modeling human cancer-induced cachexia. *Cell Rep* 2019;**28**:1612–1622.e4.
- Jogie-Brahim S, Feldman D, Oh Y. Unraveling insulin-like growth factor binding protein-3 actions in human disease. *Endocr Rev* 2009;**30**:417–437.
- Cole CL, Beck CA, Robinson D, Ye J, Mills B, Gerber SA, et al. Dual energy X-ray absorptiometry (DEXA) as a longitudinal outcome measure of cancer-related muscle wasting in mice. *PLoS One* 2020;**15**:e0230695.
- Nywening TM, Belt BA, Cullinan DR, Panni RZ, Han BJ, Sanford DE, et al. Targeting both tumour-associated CXCR2⁺ neutrophils and CCR2⁺ macrophages disrupts myeloid recruitment and improves chemotherapeutic responses in pancreatic ductal adenocarcinoma. *Gut* 2018;**67**:1112–1123.
- Bachman JF, Klose A, Liu W, Paris ND, Blanc RS, Schmalz M, et al. Prepubertal skeletal muscle growth requires Pax7-expressing satellite cell-derived myonuclear contribution. *Development* 2018;**145**:dev167197.
- Kammoun M, Cassar-Malek I, Meunier B, Picard B. A simplified immunohistochemical classification of skeletal muscle fibres in mouse. *Eur J Histochem: EIJH* 2014;**58**:2254–2254.
- Chen J, Gupta AK. *Parametric Statistical Change Point Analysis: With Applications to Genetics, Medicine, and Finance*. Springer Science & Business Media; 2011.
- Zhang L, Sanagapalli S, Stoita A. Challenges in diagnosis of pancreatic cancer. *World J Gastroenterol* 2018;**24**:2047–2060.
- Sandini M, Patiño M, Ferrone CR, Alvarez-Pérez CA, Honselmann KC, Paiella S, et al. Association between changes in body composition and neoadjuvant treatment for pancreatic cancer. *JAMA Surg* 2018;**153**:809–815.
- Zhang X-M, Dou Q-L, Zeng Y, Yang Y, Cheng ASK, Zhang W-W. Sarcopenia as a predictor of mortality in women with breast cancer: a meta-analysis and systematic review. *BMC Cancer* 2020;**20**:172–172.
- Bozzetti F. Forcing the vicious circle: sarcopenia increases toxicity, decreases response to chemotherapy and worsens with chemotherapy. *Ann Oncol* 2017;**28**:2107–2118.
- Fearon K, Strasser F, Anker SD, Bosaeus I, Bruera E, Fainsinger RL, et al. Definition and classification of cancer cachexia: an international consensus. *Lancet Oncol* 2011;**12**:489–495.
- Johnson PF. Molecular stop signs: regulation of cell-cycle arrest by C/EBP transcription factors. *J Cell Sci* 2005;**118**:2545–2555.
- Clemmons DR. Role of IGF-binding proteins in regulating IGF responses to changes in metabolism. *J Mol Endocrinol* 2018;**61**:T139–t169.
- Varma Shrivastav S, Bhardwaj A, Pathak KA, Shrivastav A. Insulin-like growth factor binding protein-3 (IGFBP-3): unraveling the role in mediating IGF-independent effects within the cell. *Front Cell Dev Biol* 2020;**8**:8.

36. Huang XY, Huang ZL, Yang JH, Xu YH, Sun JS, Zheng Q, et al. Pancreatic cancer cell-derived IGFBP-3 contributes to muscle wasting. *J Exp Clin Cancer Res* 2016;**35**:46.
37. Xue A, Scarlett CJ, Jackson CJ, Allen BJ, Smith RC. Prognostic significance of growth factors and the urokinase-type plasminogen activator system in pancreatic ductal adenocarcinoma. *Pancreas* 2008;**36**:160–167.
38. Hansel DE, Rahman A, House M, Ashfaq R, Berg K, Yeo CJ, et al. Met proto-oncogene and insulin-like growth factor binding protein 3 overexpression correlates with metastatic ability in well-differentiated pancreatic endocrine neoplasms. *Clin Cancer Res* 2004;**10**:6152–6158.
39. Yoneyama T, Ohtsuki S, Honda K, Kobayashi M, Iwasaki M, Uchida Y, et al. Identification of IGFBP2 and IGFBP3 as compensatory biomarkers for CA19-9 in early-stage pancreatic cancer using a combination of antibody-based and LC-MS/MS-based proteomics. *PLoS One* 2016;**11**:e0161009.
40. Hogan KA, Cho DS, Arneson PC, Samani A, Palines P, Yang Y, et al. Tumor-derived cytokines impair myogenesis and alter the skeletal muscle immune microenvironment. *Cytokine* 2018;**107**:9–17.
41. Kuemmerle JF, Murthy KS, Bowers JG. IGFBP-3 activates TGF- β receptors and directly inhibits growth in human intestinal smooth muscle cells. *Am J Physiol-Gastr Liver Physiol* 2004;**287**:G795–G802.
42. Yakovenko A, Cameron M, Trevino JG. Molecular therapeutic strategies targeting pancreatic cancer induced cachexia. *World J Gastrointestinal Surg* 2018;**10**:95–106.
43. Jennische E, Hall CM. Expression and localisation of IGF-binding protein mRNAs in regenerating rat skeletal muscle. *APMIS* 2000;**108**:747–755.
44. Judge SM, Nosacka RL, Delitto D, Gerber MH, Cameron ME, Trevino JG, et al. Skeletal muscle fibrosis in pancreatic cancer patients with respect to survival. *JNCI Cancer Spectr* 2018;**2**:pky043.
45. Addison O, Marcus RL, Lastayo PC, Ryan AS. Intermuscular fat: a review of the consequences and causes. *Int J Endocrinol* 2014;**2014**:309570.
46. Poff AM, Ari C, Arnold P, Seyfried TN, D'Agostino DP. Ketone supplementation decreases tumor cell viability and prolongs survival of mice with metastatic cancer. *Int J Cancer* 2014;**135**:1711–1720.